geologica**acta**

The active fault belts in eastern Tibet margin inferred using magnetotellurics

G. ZHAO [1] [*] L. WANG [1] X. CHEN [1] J. TANG [1] Z. WAN [1] Y. ZHAN [1] Q. XIAO [1] J. CAI [1] J. ZHANG [2] and J. WANG [1]

[1] **Institute of Geology, China Earthquake Administration**
Beijing 100029, China

[2] **Earthquake Administration of Shandong Province**
Jinan 250014, China

* corresponding author E-mail: zhaogz@ies.ac.cn

──┤ A B S T R A C T ├──

A magnetotelluric (MT) sounding has been carried out in the eastern margin of the Tibetan plateau. The survey line is about 145 km long, trending in NEE direction and crossing the Daliangshan block in the eastern edge of the Tibetan plateau. The field measurements acquired effective data of 68 sites. Through data processing and a 2-D inversion with consideration of topography, a 2-D electrical structure model of crust and upper mantle was constructed. The structure reveals that there is a deep electrical boundary between the Daliangshan block in the west and Sichuan block in the east. West to the boundary, the crust has a relatively low resistivity with respect to the east and can be divided into three layers, the middle layer has low-resistivity with a minimum of 3-10 $\Omega \cdot m$, presumably associated with partial melt and/or salty fluids. Beneath the intersection area of the Anninghe fault, the Xianshuihe fault and the Longmenshan fault, which the MT profile crosses, the faults are separated into upper and lower sections. The upper section exhibits a nearly vertical low-resistivity zone in the upper crust, and the lower section manifests an electrical boundary in the lower crust and upper mantle. Other faults in the Daliangshan block are either nearly vertical low-resistivity zones or electrical boundaries. It is suggested that the formation of the low-resistivity layer in the middle crust is associated with the southeastward motion of the eastern margin of the Tibetan plateau, clockwise rotation of the Chuandian (Sichuan-Yunnan) block, and the westward obstruction from the Sichuan block in Huanan terrain. Seismicity, including the M 8.0 Wenchuan earthquake in the study area, is discussed.

KEYWORDS | **Eastern margin of Tibetan plateau. Active fault. Electrical structure. Channel flow. Wenchuan Earthquake.**

INTRODUCTION

The eastern margin of the Tibetan plateau, geographically covering the Sichuan (Chuan) and Yunnan (Dian) provinces in China, is one of the areas with the most intensive crustal deformation and earthquakes in the world (Fig. 1). Numerous studies have been done on active faults and their relationships with seismicity of this area (Clark et al., 2000, Deng et al., 1994; Li et al., 2003; Lu et al., 1989; Peng and Zhou, 1991; Roger et al., 1995; Royden et al., 1997; Sun et al., 2003; Teng, 1994; Wang et al., 2007; Xu et al., 1992; Zhang et al., 2003; Zhang et al., 2004; Zhu A et al., 2005; Zhu J et al., 2005; Zhu et al., 2004; Zhao et al., 2008, 2009).

In the eastern margin of the Tibetan plateau, there is a rhombic terrain, the Chuan-Dian (Sichuan-Yunnan) block (CDb) encompassed by active faults with a NNW trending long axis. East to the block, from north to south, are the Xianshuihe fault (XSHf), the Anninghe fault (ANHf), and the Zemuhe fault (ZMHf), adjoining the Songpan-Ganzi block (SGb) and the Daliangshan block (DLSb) in Huanan (South China) terrain (HNb). In the west, lie the Jinshajiang faults (JSJf) and the Honghe faults (HHf) neighboring upon the Qaingtang block (QTb) and the Diannan (south Yunnan) block (DNb) (Fig.1) (Bureau of Geology, 1991; Deng et al., 1994; Ma, 1989; Wen et al., 2003; Xu et al., 2003, 2005; Zhang et al., 2003).
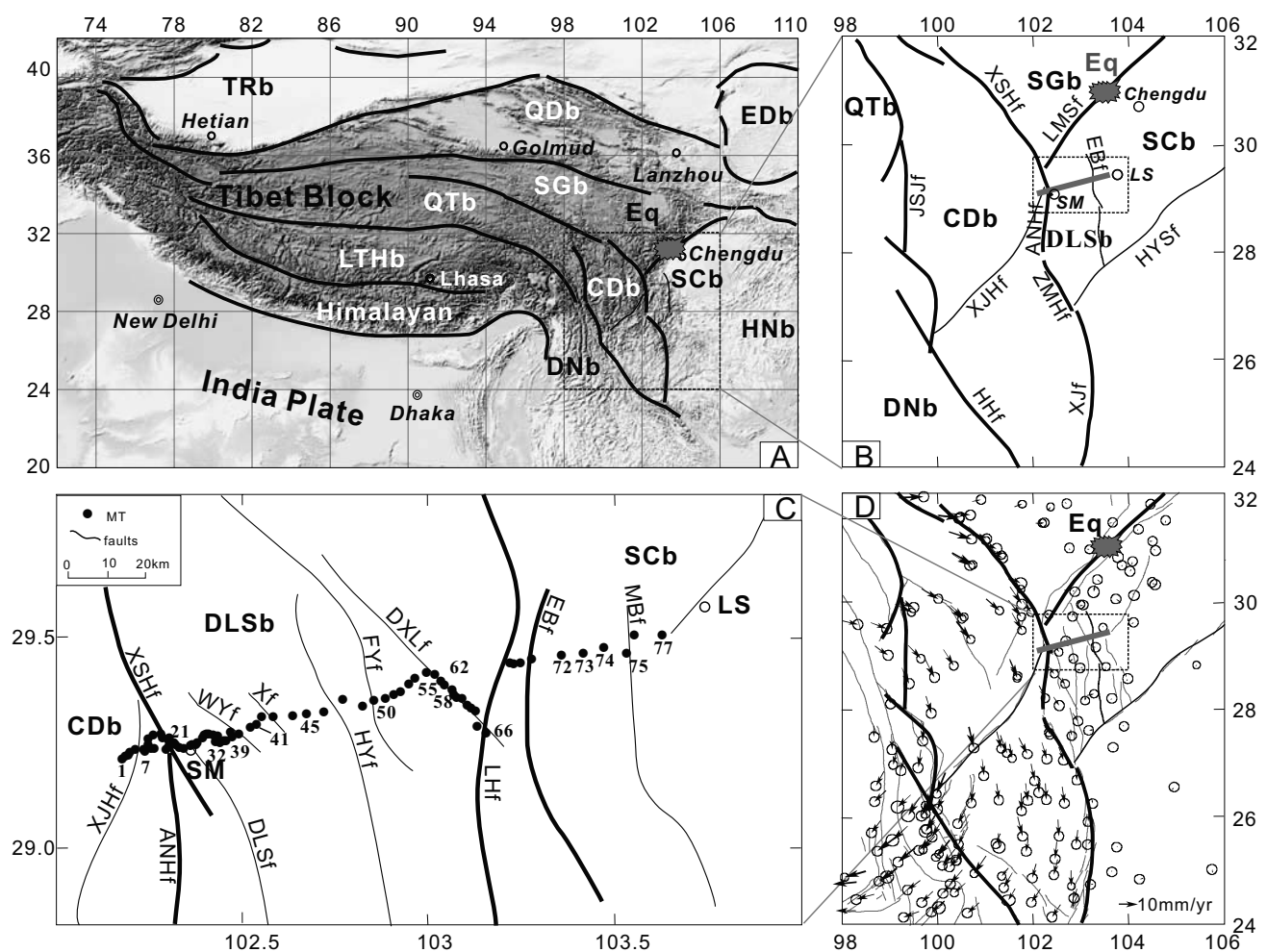

FIGURE 1 | **Tectonic setting around the Shimian-Leshan MT line (SLp). A)** Regional tectonics of the Tibet plateau (including Himalayan, LTHb, QTb, SGb, QDb and CDb) and its surrounding. **B)** Tectonics around CDb and DLSb (after Xu et al., 2005). Thick line shows Shimian-Leshan MT line (SLp). **C)** Location of MT line and the relation with some faults and blocks. **D)** GPS velocity field with respect to the HNb (after Wang et al., 2008). Cities (space circles): LS-Leshan, SM-Shimian and other full names (e.g., Chengdu city). Block names: TRb-Tarim block (hereafter "block" is omitted), QDb-Qidam, SGb-Songpan-Ganzi, QTb-Qiangtang, LTHb-Lhasa, DNb-Diannan, EDb-Erdos, SCb-Sichuan, HNb-Huanan (or South China), CDb-Chuandian, DLSb-Daliangshan (in between CDb and SCb). Fault names: XSHb-Xianshuihe faults (hereafter "faults" is omitted), ANHf-Anninghe, ZMHf-Zemuhe, XJf-Xiaojiang, JSJf-Jinshajiang, XJHf-Xiaojinhe, HHf-Honghe, LMSf-Longmenshan, EBf-Ebian, HYSf-Huayingshan. DLSf-Daliangshan, WYf-Wanyuan, HYf-Hanyuan, FYf-Fengyi, DXLf-Daxiangling, LHf-Liujiang-Hongxi, MBf-Mabian, Xf-found in this paper. Exploded solid mark: Wenchuan earthquakes epicenter on May 12, 2008.

The nearly NS striking Daliangshan block (DLSb) confined by active faults, about 100 km wide in the east-west direction, is situated east of the CDb as a part of the HNb. West of the DLSb are the ANHf and the ZMHf, bordering on the CDb; and, in the east lie the Liujiang-Hongxi faults (LHf) and the Ebian faults (EBf) next to the Sichuan block (SCb) in the HNb (Fig.1).

Geological studies show that the western boundary faults of the CDb are dominated by dextral strike-slip motion, while the eastern boundary faults (XSHf, ANHf and ZMHf) exhibited tensile motion during early Pleistocene time and sinistral strike-slip motion by late Pleistocene time (Wang et al., 1996). South and north of the intersection area of the XSHf and ANHf, active faults move quite differently. In the north, the XSHf is of sinistral strike-slip with a rate of 12mm/yr, and in the south, the ANHf and the ZMHf have both sinistral strike-slip with a rate of 6~8 mm/yr and eastward thrust motion (Shen et al., 2005; Xu et al., 2005; Zhang et al., 2003). The study also indicates that the CDb experiences a southeastward motion and clockwise rotation simultaneously, and the total amount of the rotation since the Oligocene or the early Miocene is as much as 30-48° (Xu et al., 2003).

Seismicity differs north and south of the intersection area. In the north, the northern and middle sections of the XSHf have frequent major earthquakes, with 8 events of magnitude 7 or greater having occurred since 1480. While in the south, along the ANHf and the ZMHf, only 1 or 2 major earthquakes have been recorded, although small events of magnitude 0.1-4.9 are more abundant here than along the XSHf. The sources of these small shocks are confined to the depth range 0-15 km and concentrated on the faults and their adjacent areas (Wen et al., 2003; Zhu A et al., 2005).

The Songpan-Ganzi block (SGb) is located north and northeast of the CDb. The southeastern boundary of the SGb is the Longmenshan fault (LMSf) striking in a NE direction and adjoining the Sichuan block (SCb) (Fig.1). The Wenchuan Ms 8.0 earthquake occurred in the middle section of the LMSf on May 12, 2008. Southeastward motion of the SGb in the middle section of the LMSf with a rate of merely 1 mm/yr or less has been detected by GPS in recent years and is perpendicular to the strike direction of the LMSf (Fig.1D) (Shen et al., 2005; Wang et al., 2008). Sinistral strike-slip and dextral strike-slip motions with similar rates to those in the middle section can be observed in southwestern and northeastern sections of the LMSf, respectively.

Historical earthquakes of M < 4.9 occurred in the middle section more frequently than in the southwestern and northeastern sections, but less frequently than in the ANHf

and the ZMHf. There were fewer stronger earthquakes that occurred during the last centuries in the LMSf (Wen et al., 2003; Chen et al., 2007; Xu et al., 2008; Zhang et al., 2008). Investigating the crustal structure beneath the LMSf and the neighboring regions will help in understanding the generation of the 2008 Wenchuan Ms 8.0 event.

The crustal structures on the east and west side of the Daliangshan block (DLSb) exhibit distinct features. The DLSb is of a transitional zone in the eastern margin of the Tibetan plateau. The crust is approximately 63 km thick in the west and 45 km thick in the east. Both the average velocity (6.25 km/s) of crust and the velocity (7.75 km/s) of the uppermost upper mantle in the west are evidently lower than those in the east (6.45-6.50 km/s and 8.00-8.20 km/s, respectively) (Wang et al., 2007). In the west, there is an 8-10 km thick low-velocity layer at depth 15 km, while it does not exist in the east. A nearly NS-oriented intense gradient zone of Bouguer gravity anomalies passes through the DLSb being from $-200 \cdot 10^{-5}$ m/s^2 in the east of DLSb to $-400 \cdot 10^{-5}$ m/s^2 in the west for only about 100 km (Lou and Wang, 2005).

Although a great number of studies have been done on active faults and seismicity in this area, as briefly presented above, the deep structures of these faults remain unclear (Lu et al., 1989; Sun et al., 2003; Teng, 1994; Wang et al., 2007; Zhang and Klemperer, 2005; Zhu J et al., 2005).

In recent years we have carried out a magnetotelluric (MT) survey in this area to probe the electrical structure of the crust and upper mantle. The MT line, about 145 km long, called the Shimian-Leshan profile (SLp), is in a nearly NEE direction (about N80°E) perpendicular to the regional tectonic strike of the study area. It starts from the east of the diamond-shaped CDb which situates in the west of the intersection area of the XSHf and the ANHf, extends eastward across the DLSb and ends at the SCb. This profile also crosses other faults in the DLSb (Fig.1).

MT DATA

Remote reference MT data were collected at 77 sites along the profile. In the west section of the profile, namely near the XSHf and the ANHf faults, site spacing is relatively small with a minimum of less than 1 km; and in the east section, site spacing is fairly large with an average of several km. Two electrical components (Ex, Ey) and three magnetic components (Hx, Hy and Hz) were measured along the north, east and downward directions, denoted by x, y and z, respectively. The robust method was used in data processing (Jiang et al., 1993) and visualization software for MT data was employed in analysis (Chen et al., 2004).

Due to disturbance from some small hydroelectrical power stations in the survey area and serious topographic relief along the profile, the measurements at some sites contained major errors. Therefore, we selected data from 68 sites of good quality for this study. The frequencies of these data range from 320 Hz - 0.0005 Hz.

Data quality is improved by using MT remote reference (RR) in data processing (Gamble et al., 1979). The enhancement of signal over noise for apparent resistivity curves seems to be more obvious than for phase curves. In more than half of the sites, depending on the site, the improvement of using RR appears in either higher, middle or lower frequency bands, but it is not as obvious for the other sites. Figure 2 displays the result of site 71 by using remote reference. It demonstrates that the divergence of apparent resistivity curves at a frequency of around 0.1 Hz is reduced by using the remote reference MT technique in data processing.

Figure 3 illustrates the apparent resistivities, impedance phases and Swift skewness (Swift, 1967) for sites 10, 45, 58 and 76, which are somewhat representative. It illustrates that in general the curves are fairly continuous, though some frequency bands of apparent resistivities and phases for some sites have rather significant errors. At most of the sites, the morphology of the apparent resistivity curves indicates that from the surface downwards, the resistivity is low near the surface, increases towards the upper crust, decreases in the middle crust and rises again thereafter.

In addition, the impedance tensor decomposition technique (Bahr, 1988) was applied to the analysis of the data. No major difference of parameters, e.g., apparent resistivity and phase, was found for most sites after the application of tensor decomposition. This implies that most
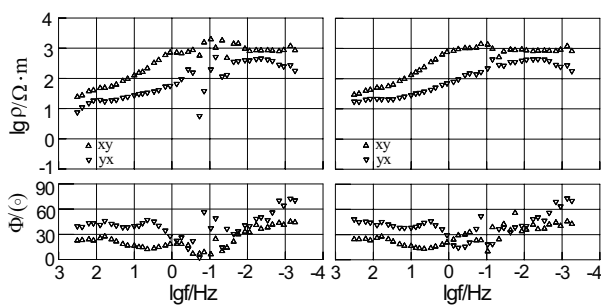
sites were not significantly affected by local distortion. The following discussion is mainly based on the parameters calculated using the Swift algorithm (Swift, 1967).

The values of the Swift skewness on the main frequencies for most sites are less than 0.3 required by 2-D electrical structure (Bahr, 1988). However for a few sites, skewness values are bigger than 0.3, e.g., for frequencies lower than 0.1 Hz at site 10 (Fig.3), which may be caused by data error or something else. For most sites, the azimuths of principal electrical axes on main frequencies are around 0° (Fig. 4) which means that they align approximately with regional tectonics (perpendicular to the profile trend)(Fig. 1).

We considered the following features for most sites: 1) the principal electrical axes point approximately NS (the tectonic strike) or nearly EW (the dipping direction); 2) Swift skewness less than 0.3 which is necessary (although not sufficient, Ledo et al., 2002; Martí et al., 2005) for a 2-D model and 3) real induction vectors in the EW direction (tectonic dipping direction). Thus, we suggest that the electrical structure of the study area strikes roughly in a NS direction, perpendicular to the trend of the MT profile, and can be approximated by a 2-D model along the MT profile (Zhan et al., 1999; Zhao et al., 1990, 2005).

TWO-DIMENSIONAL GEOELECTRICAL MODEL

2-D inversions were made using the profile data by using the RRI (Rapid Relaxation Inversion, Smith and Booker, 1991) and NLCG (NonLinear Conjugate Gradients algorithm, Rodi and Mackie, 2001) methods. The final 2-D
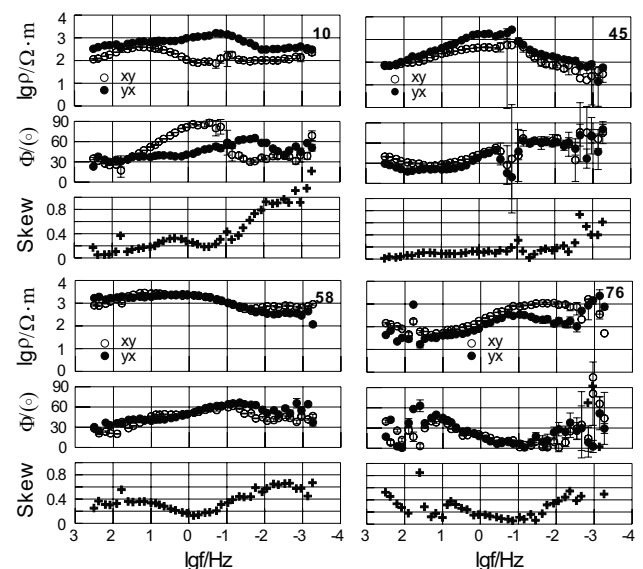
FIGURE 2 | **Comparison of analysis results for site 71 using the remote reference MT method (RR). Left charts show apparent resistivity and impedance phase without using RR. Right charts show those using RR. Upper charts are apparent resistivities, where ordinates are resistivity (Ω·m) in logarithmic scale. Lower charts are impedance phases, where ordinates are degrees. Abscissas are frequencies (Hz). xy and yx denote the data (apparent resistivity and impedance phase) for the electrical field components, perpendicular and parallel to the line direction (TE and TM polarizations), respectively.**

FIGURE 3 | **Observed curve sets displayed in columns for sites 10, 45, 58 and 76 located from W to E. xy and yx are the same as in FIGURE 2.**
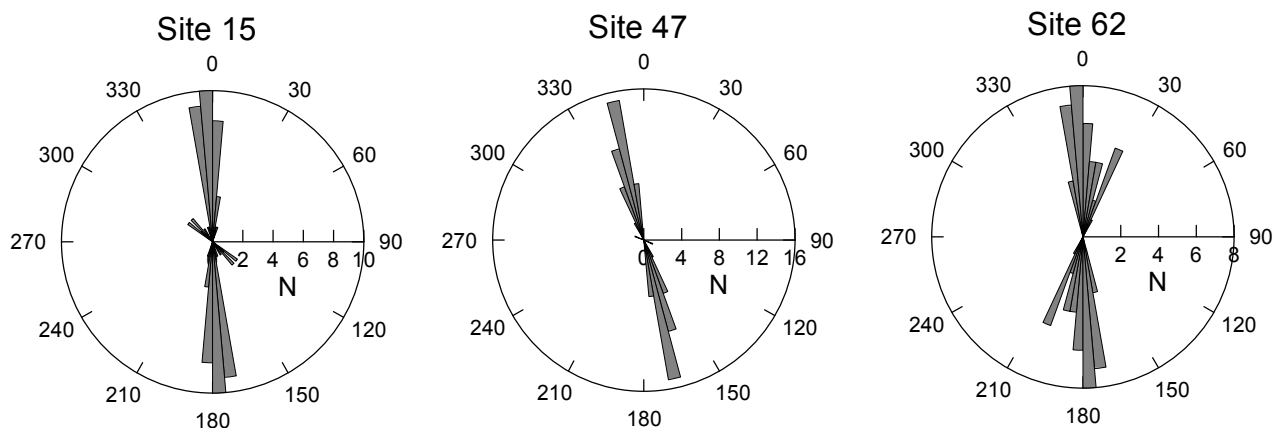
FIGURE 4 | **Optimum Swift rotation angles for sites 15, 47 and 62, shown as rose schemes. The 0° angle represents north, along which horizontal electric (Ex) and magnetic (Hx) fields are measured. In each site scheme the grey regions connected with the center of the circle indicate azimuths of principal electrical axes and the number (N) of frequencies in the azimuths.**

model presented in this paper (Fig. 5, Table 1) is from the NLCG method.

Prior to the inversion, the data were rotated to be aligned with the directions parallel to the survey line denoted by yx (TM polarization mode) and perpendicular to the survey line denoted by xy (TE polarization mode). Considering topographic relief and different site spacing along the survey line, the profile was first divided into four segments for inversion which corresponded to site numbers 01-21, 20-43, 42-60 and 58-77. When the inversion result of each segment met the fitting requirement, the final models of these four segments were merged to form the initial model for the further inversion of the whole profile.

Vertical mesh sizes are 10 meters in the first row of the model and increase gradually downward with ratios

between 1.2 and 2. The total number of vertical rows is 89. Horizontally, the model is divided into a total of 132 columns, ensuring that there is at least one column separating every two adjoining sites. Three kinds of data, i.e., TM polarization data, TE polarization data and combined TM and TE data, were used for the inversion calculation. The inversion using the TM data shows better data fitting than the other two kinds of data and thus TM data is used in this paper.

In the inversion, the elevation of every site was incorporated into the model grid (Chen, 2000). Some of the abrupt resistivity and/or phase data points are ignored for inversion. The static shift appears at 20 sites and is automatically corrected in the inversion process, and the predesigned correction factors for some sites are included.
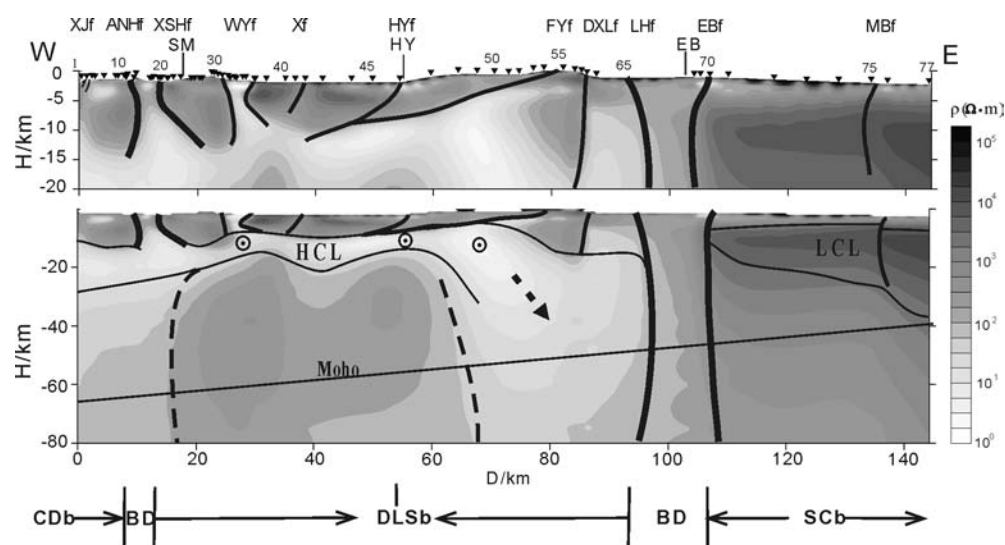

FIGURE 5 | **Two-D electrical structure along the Shimian-Leshan profile. Upper: depth range 0 - 20 km. Lower: depth range 0 - 80 km, with enlarged horizontal scale. The arrow and circles with dots in the low-resistivity layer of the middle crust denote the motion direction of the low-resistivity layer, which is supported by the real-part induction vector (not shown). The grey scale contains resistivity values. The reversed triangles along the uppermost line denote sites. BD= boundary zone. HCL= High conductivity layer in the crust. LCL= Low conductivity (resistive) layer. City names: SM= Shimian. HY= Hanyuan. EB= Ebian. Xf= Electric boundary, assumed to be a fault. Marks of faults and blocks are the same as the figures above, with fault names on the top.**

TABLE 1 | **Crustal electrical properties for different tectonic units along the SLf profile.**

Tectonic units	CDb	XSHf-ANHf	DLSb	LHf-EBf	SCb
Upper crust	$10^2 \sim 10^3$ Ω·m, ~15 km thick	Upper section: low resistivity, 3~5 km width	$10^2 \sim 10^3$ Ω·m, ~15 km thick, inner wedge-shaped body	Steep electric boundary zone	>10^3 Ω·m, max. values at depth ~15km, no HCL
HCL	$10^0 \sim 10^1$ Ω·m		$10^0 \sim 10^1$ Ω·m, 10~30- 40 km thick, eastward underthrust		
		Lower section: electrical			Resistivity decreases with increasing depth
Below HCL	$10^1 \sim 10^2$ Ω·m	boundary	two subsections in horizon		

A sketch of final static correction factors of apparent resistivities for each site is displayed in Fig. 6.

Figure 7 shows pseudosections of observed TM apparent resistivities and phases and calculated responses of the final model. As shown in Fig. 8, the data fitting errors are generally less than 12% for apparent resistivity and less than 12º for phase, implying that the final model is acceptable.

As shown in Fig. 5 and in Table 1, the resultant 2-D model of the electrical structure along the profile is divided into two sections, the boundary between the two lying just between the DLSb and the SCb. The electrical resistivities west of the boundary are generally lower than those to the east.

West of the boundary, the electrical structure of the crust is comprised of three layers. The upper crust is the layer of high-resistivity with values of several hundred Ω·m up to several thousand Ω·m. This high-resistivity

FIGURE 6 | **Factors of static correction for every site along the profile. Ordinates are scaling coefficients of correction. Number 1.0 means no correction. Abscissas are the distances along the profile.**

layer resembling a flat wedge-shaped body is about 15 km thick near the western end of the profile, becomes thinner eastward and vanishes around the Fengyi fault (FYf).

Below this high-resistivity layer is the middle crustal low-resistivity zone of between 1 and 30 Ω·m (HCL). The thickness of the layer is about 20 km at the western end of the profile, thins eastward and reaches the minimum 10 km near the Hanyuan faults (HYf). Further eastward, this low-resistivity layer becomes thicker again with maximum values of 30 - 40 km and seems to underthrust toward the east.

Beneath the low-resistivity middle crust, the lower crust and upper mantle get more resistive with depth. This lower part of the model along the profile can be divided into three subsections laterally (see the discontinuous line in Fig. 5). The middle section lies roughly between the Xianshuihe-Anninghe fault (XSHf-ANHf) and the HYf and has higher resistivity than the other two subsections.

East of the boundary, the resistivity of the crust is apparently higher than that to the west, reaching the maximum value of tens of hundreds of Ω·m at a depth of about 15 km, without a low-resistivity layer in the crust. Below this mostly high resistive zone, the resistivity reduces gradually with increasing depth.

It should be noted that the section in the profile from site 59 to 66 deviates from the general trend (NNE) of the profile but is perpendicular to the local structural orientation. Hence, the data of this section was inverted separately, and the result exhibits the existing electrical boundary in agreement with that from the inversion of the entire profile.
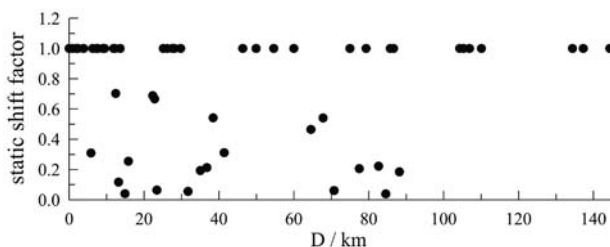
Figure 9 shows the apparent resistivity curves of TM polarization for three sites, 42, 45 and 48 from west to east located in the Daliangshan block (DLSb). The major portions of these three curves are similar to each other, with close frequencies corresponding to their maximums, of which the values reduce from site 42 to 48, namely from west to east. It means that the depth of the low-resistivity layer in the middle crust becomes smaller from west to east, in agreement with the 2-D electrical structure. In addition, the right branches of the apparent resistivity curves for sites 42 and 45 exhibit that the media below the low-resistivity layer in the middle crust becomes more resistive downward. This is in accordance with the variation tendency of the right branches of apparent resistivity curves to decrease at first and then increase again with decreasing frequencies. This decrease at the right branch of the curve for site 48 is probably due to the thin high-resistivity layer in the upper crust and the thick low-resistivity layer in the middle crust beneath this site. These curves (Fig. 9) demonstrate that the suggested three-layer crustal structure geoelectrical model is convincing.

DEEP STRUCTURE OF ACTIVE FAULTS

Many studies on active faults in the eastern margin of the Tibetan plateau (Deng et al., 1994; Ma, 1989; Wen and Yi, 2003; Xu et al., 2003, 2005, 2008; Zhang et al., 2003, 2008) provide valuable help in interpreting the deep electrical structures of these discontinuities from the MT survey in this area. Most of these faults are experiencing both sinistral strike-slip and thrust motions, which manifest boundaries of changing resistivity, steeply changing gradient zones or low-resistivity anomaly zones associated with fractured rock in the electrical structural profile.

In light of the electrical structure along the Shimian-Leshan profile presented in this paper, we have estimated the deep structures of the faults crossed by the MT line.

Near km 100 in the profile (Fig. 5), there is an electrical boundary across which the resistivity suffers the largest change. This boundary is in accord with the positions of the LHf and the EBf between the DLSb and the SCb. The relatively steep electrical boundary can help with interpretation of left-lateral strike-slip motions on these faults, and supports the inference that the DLSb is moving southward with respect to the SCb.

Geologically, the XSHf and the ANHf are the divisional zones between the CDb and the Songpan-Ganzi block (SGb), and between the CDb and the DLSb, respectively, which are deep and large in scale, with sinistral strike-slip (Bureau of Geology, 1991; Ma, 1989; Wang et al., 1996; Xu et al., 1992; Zhang et al., 2003). The electrical structure (Fig. 5) shows that these faults are cut into two sections by a low-resistivity layer in the middle crust. The upper sections of the faults manifest nearly vertical anomalous zones of low-resistivity with a width of 3 - 5 km, within which the media are characterized by low-resistivity (around tens of $\Omega \cdot m$) in large contrast to the highly resistive media (over a thousand $\Omega \cdot m$) outside the faults. The lower sections of the faults coincide with the nearly vertical electrical boundaries in the lower crust and upper mantle, with higher resistivity in the east than in the west.

Available geological data (Bureau of Geology, 1991) suggest that the Wanyuan fault (WYf) is of a small scale in this area, surrounded by much exposed granite. Theoretically, the media around this fault should be highly resistive. However, the actual electrical structure indicates that around the WYf in the upper crust a relatively low-resistivity zone exists which is nearly vertical, about several km wide. The bottom of the zone is near the top of the low-resistivity in the middle crust,
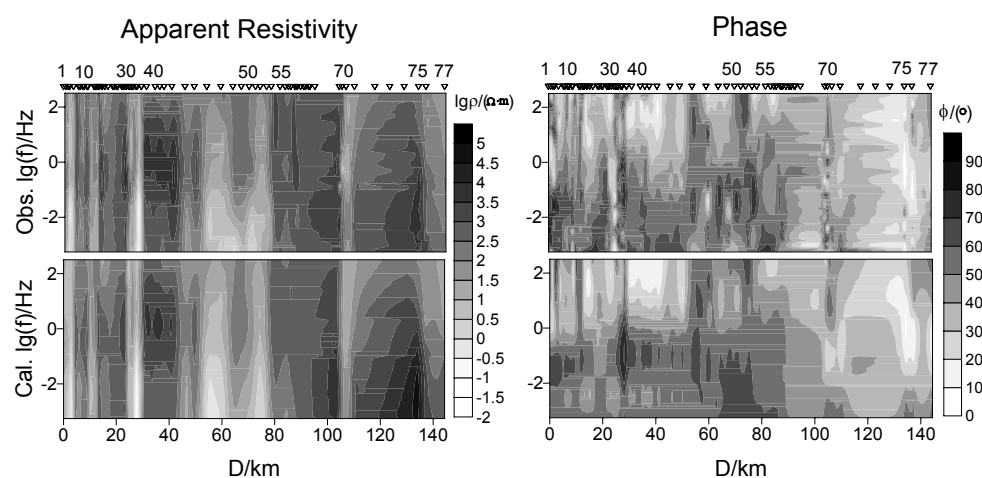

FIGURE 7 | **Pseudosections of apparent resistivity (left) and phase (right) for TM polarization data along the profile. Upper row: observed data. Lower row: model data. Ordinates are logarithms of frequencies. Abscissas are the distances along the profile. The grey scales denote logarithms of resistivity and degrees of phase. Reversed triangles with numbers along the uppermost line denote site identification.**

like the case beneath the intersection area of the XSHf - ANHf mentioned previously. This vertical zone of low-resistivity could be interpreted as a strike-slip fault, and might give new insight into the existing WYf from the geological survey.

In the electrical structure model, other faults within the Daliangshan block (DLSb), e.g., the HYf and the FYf, are represented by westward dipping electrical boundaries. Both faults meet and disappear at the top of the low-resistivity layer in the middle crust, confining an inner wedge-shaped body tilting to the west in the profile. The geometric patterns of these two faults and the inner wedge-shaped body may be associated with the ubiquitous structures of thrust and detachment in this area (Xu et al., 1992; Wang et al., 1996).

In the block between the WYf and the HYf, the fault which was suggested by geological data (Bureau of Geology, 1991) is not evident. But, the electrical structure reveals a low-resistivity boundary near the center of this block the lower section of which diminishes at the uppermost low-resistivity layer in the middle crust. We speculate that this electrical boundary could be the trace of a fault, which we refer to as Xf, which coincides with the source distribution of recently relocated small events (M<4.9) (Zhu A, 2007, pers. comm.).

The electrical structure also shows that the Daxiangling fault (DXLf) in the Daliangshan block (DLSb) and the Mabian fault (MBf) in the SCb manifest nearly vertical electrical boundaries, along which many small concentrated earthquakes occurred (Zhu A, 2007, pers. comm.).
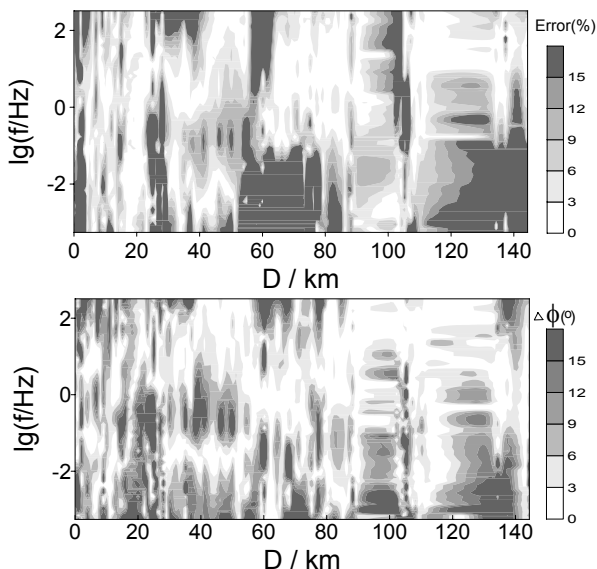

FIGURE 8 | Contours of relative fitting errors of apparent resistivity in percentage (upper) and phase in degrees (lower) along the profile. Coordinates are the same as in FIGURE 5.
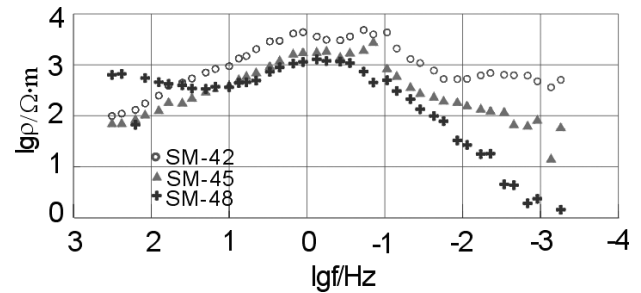

FIGURE 9 | Apparent resistivity curves from TM polarization data of sites 42, 45 and 48. Ordinates denote logarithms of apparent resistivity ($\Omega \cdot m$). Abscissas denote frequency (Hz).

CONCLUSIONS AND DISCUSSION

1) Three segments of the profile

The Shimian-Leshan electrical structural profile can be divided into three sections, corresponding, from W to E, to the CDb, the Daliangshan block (DLSb) and the SCb (Fig. 5 and Table 1). They are separated by nearly vertical electrical boundaries or steep strike-slip faults. The SCb is a stable tectonic block, with an underlying crust of high resistivity. The crust of the other two blocks has relatively low resistivity and is comprised of three layers, among which the middle layer (middle crust) is a relatively low-resistivity horizon. Within the Daliangshan block (DLSb) the faults are characterized by thrust or steep strike-slip motion. Within the XSHf - ANHf and the WYf, the resistivity is lower than tens of $\Omega \cdot m$. It was probably caused by rock fragmentation, pore increase and fluid infiltration during strike-slip of the faults. This speculation is supported by the ductile shear belts and mylonite along the XSHf - ANHf (Wang et al., 1996).

2) Partial melting in the middle crust

Under dry conditions, the rock resistivity in the crust can be up to $10^5 \Omega \cdot m$ or more. The investigation in the southern edge of the Tibetan plateau found that a low-resistivity zone (3 - 10 $\Omega \cdot m$) exists at a depth of 15 km, which was speculated to be partial melt of leucogranite. It was suggested that the eastern margin of the Tibetan plateau also has similiar tectonic and dynamic settings (Chen et al., 1996; Clark and Royden, 2000; Li et al., 2003; Liu et al., 2005; Nelson et al., 1996; Pham et al., 1986; Renner et al., 2000; Rosenberg and Handy, 2005; Royden et al., 1997; Schoenbohm et al., 2006; Unsworth et al., 2005; Wei et al., 2001; Yuan et al., 2006).

In this study area, the eastern rim of Tibet, there are many well developed crustal detachments (Teng, 1994; Wang et al., 1996; Xu et al., 1992). Northwest of the MT profile, approximately 50 km away, a granite sheet of 12.8

Ma age has been observed at the Gongga Mountains. On the surface, there are many hot springs (Roger et al., 1995; Sun et al., 2007; Zhang et al., 2004). The geothermal study suggests that the temperature at depths 15 - 20 km is about 500 - 600°C in this region (Zhu J et al., 2005). The geologic and geothermal conditions in this area, similar to those in southern Tibet, can draw an inference that several bodies of 3 - 10 $\Omega \cdot$m in the middle crust along the MT profile may contain partial melt of 10% content and some quantity of salty fluids.

3) 'Channel flow' in the crust of the eastern Tibet margin

The low-resistivity layer in the middle crust is generally easy to flow due to the fact that it might contain media of low rheological parameters which has been called the channel flow horizon (Clark and Royden, 2000; Gaillard et al., 2004; Grujic, 2006; Harris, 2007; Hilley et al., 2005; Medvedev and Beaumont, 2006; Royden et al., 1997; Schoenbohm et al., 2006; Unsworth et al., 2005). The low-resistivity layer in the middle crust inferred from the MT data in this area is presumably a channel flow horizon, which was formed by two factors: the east- and southward movement of the Tibet block in the eastern margin of the Tibetan plateau; and the big pressure difference caused by large elevation contrast (about 3000 m) (Ma, 1989) between the eastern edge of the plateau and its outside terrain. As this motion was obstructed by the SCb in the HNb in the east, it turned downward as well as toward the southeast (Fig. 1 and Fig. 5).

The existing channel flow horizon can decouple the upper crust from the lower crust, and probably imposes traction upon the upper crust (Zhu and Shi, 2004). The brittle high-resistivity upper crust may thin to some extent leading to rising of the surface, within which sinistral and thrust faults occur. The integrated effect of these motions and deformation of the crust is likely the reason that the crustal thickness of this area reduces rapidly from 63 km in the west to 45 km in the east (Wang et al., 2007).

4) Relationship between seismicity and electrical structure

In the middle crust, the rocks of low-resistivity are of low strength and easy to suffer plastic deformation or to flow, thus they are not favorable for accumulation of stress and seismic energy. While in the brittle and highly resistive upper crust, energy for tectonic motion and deformation can build up. In the area of the MT profile, intense crustal motion and deformation, as well as flow of the low-resistivity layer in the crust, provide conditions for accumulation and release of seismic energy. In particular, the brittle crust is the locus of strain building up while the

low-resistivity layer in the middle crust can help energy release and prevent major earthquakes. Therefore the study area of the profile is characterized by frequent small earthquakes and occasional major events, differing from the middle and northern sections of the XSHf. Meanwhile, moderate- and small-magnitude earthquakes are confined to the upper crust at depths less than 15 km in this area. For instance, earthquakes occur at the WYf, at the MBf, and at the intersection of the XSHf and the ANHf, forming the nest of small shocks (Wen and Yi, 2003; Xu et al., 2005; Zhu A et al., 2005).

The Wenchuan Ms 8.0 earthquake on 12 May 2008 occurred in the center section of the Longmenshan fault (LMSf) which starts from the intersection area of the ANHf, the XSHf and the LMSf and runs northeastward for about 500 km (Fig. 1). Although the LMSf and the ANHf suffered similar southeastward action due to the crustal movement of the SGb and the CDb, respectively, on their west, the angles between the moving direction of these two blocks and their relative faults (LMSf and ANHf) are different. The moving of the SGb is along the direction nearly perpendicular to the LMSf strike and has a T-shaped form, while the angle between the moving direction of the CDb and the ANHf strike is about 45° or less. The stable and rigid Sichuan block (SCb) without the crustal low-resistivity layer lies southeast of the LMSf. A transition zone, the DLSb lies between the SCb and the CDb. In the area of the LMSf, the SGb meets the frontal obstruction of the SCb such that it is difficult to move and/or deform but prone to accumulation of stress. Thus, a smaller deformation rate (merely around 1 mm/yr) (Fig. 1D) and weaker seismicity appear in this area. However, in the area of the ANHf, the movement of the CDb and the ANHf strike form an acute angle, because of this, the movement of the CDb is simpler than that of the SGb Thus, the southeastward motion of the CDb under push of the QTb on the west causes the southeastward flow of the crustal low resistivity layer which cuts the ANHf slantwise and enters the DLSb and then turns to a southward direction beneath the DLSb that is nearly parallel to the western margin of the SCb (Fig. 1 and Fig. 5). These actions cause the larger motion rates (6 ~ 8 mm/yr) and frequent medium- and small-magnitude earthquakes in the ANHf and vicinity (Shen et al., 2005; Wen and Yi, 2003; Xu et al., 2008). The Wenchuan earthquake occurred in the center of the T-shaped form in the LMSf where stress is most prone to accumulate but not to release. Once the accumulated stress is larger than the rock strength, a very strong shock would take place. Therefore it was a long quiet time before the 2008 Wenchuan earthquake (Wen and Yi, 2003). Meanwhile, the significant deformation and release of seismic energy in the XSHf, the ANHf and the neighboring areas of the LMSf also aggravated the stress accumulation in the LMSf area.

The result of this study is important for understanding the active faults and deep structures in the eastern margin of the Tibetan plateau, particularly because it not only provides evidence from the MT survey for the existence of the channel flow in the crust, but also helps to understand the earthquake activity and the preparation of strong Wenchuan earthquakes. Our analysis of other MT profiles in the eastern edge of the Tibetan plateau is ongoing, of which the preliminary results support the conclusions of this paper. Nevertheless, further studies of the MT profile presented in this work and other MT profiles remain necessary.

ACKNOWLEDGMENTS

REFERENCES

Bahr, K., 1988. Interpretation of the magnetotelluric impedance tensor: regional induction and local telluric distortion. Journal of Geophysics, 62, 119-127.

Bureau of Geology and Mineral Resources of Sichuan Province, 1991. Regional geology of Sichuan province (in Chinese). Beijing, Geological Publishing House, 567-601.

Chen, G., Ji, F., Zhou, R., Zhou, R., Xu, J., Zhou, B., Li, X., Ye, Y., 2007. Preliminary research of activity segmentation of Longmenshan fault zone since late-quaternary (in Chinese). Seismology and Geology, 29(3), 657-673.

Chen, L., Booker, J.R., Jones, A.G., Wu, N., Unsworth, M., Wei, W., Tan, H., 1996. Electrically conductive crust in southern Tibet from INDEPTH magnetotelluric surveying. Science, 274, 1694-1696.

Chen, X., 2000. On the research of the influence of terrain to MT 2D forward computation (in Chinese). Geophysical Prospecting for Petroleum, 39(3), 112-120.

Chen, X., Zhao, G., Zhan, Y., 2004. Visual window system for MT data processing and interpretation (in Chinese). Oil Geophysical Prospecting, 39(supplement), 11-16.

Clark, M., Royden, L., 2000. Topographic ooze: Building the eastern margin of Tibet by lower crustal flow. Geology, 28(8), 703-706.

Deng, Q., Chen, S., Zhao, X., 1994. Tectonics, seismicity and dynamics of Longmenshan mountain and its adjacent regions (in Chinese). Seismology and Geology, 16(4), 389-403.

Gaillard, F., Scaillet, B., Pichavant, M., 2004. Evidence for present-day leucogranite pluton growth in Tibet. Geology, 32(9), 801-804.

Gamble, T.D., Goubau, W.M., and Clark, J., 1979. Magnetotellurics with a remote magnetic reference. Geophysics, 44, 53-68.

Grujic, D., 2006. Channel flow and continental collision tectonics: an overview. London, Geological Society, 268, 25-37.

Harris, N., 2007. Channel flow and the Himalayan–Tibetan orogen: a critical review. Journal of the Geological Society, 164, 511-523.

Hilley, G.E., Bürgmann, R., Zhang, P., Molnar, P., 2005. Bayesian inference of plastosphere viscosities near the Kunlun Fault, northern Tibet. Geophysical Research Letters, 32(1), L01302.1-L01302.4.

Jiang, Z., Liu, G., Sun, J., 1993. Robust estimation and its application in the MT data processing. In: Liu, G. et al. (eds). Investigation and Application of Electromagnetic Methods (in Chinese). Beijing, Seismological Press, 60-69.

Ledo, J., Queralt, P., Martí, A., Jones, A.G., 2002. Two-dimensional interpretation of three-dimensional magnetotelluric data: an example of limitations and resolution. Geophysical Journal International, 150, 127-139.

Li, S., Unsworth, M., Booker, J.R., Wei, W., Tan, H., Jones, A.G., 2003. Partial melt or aqueous fluid in the mid-crust of Southern Tibet? Constraints from INDEPTH magnetotelluric data. Geophysical Journal International, 153, 289-304.

Li, T., Deng, Z., Lu, Y., 2003. Research on the crustal deformation data related to characteristics of strong earthquake (MS\610) distribution in the Area of Chuandian (Sichuan-Yunnan), China (in Chinese). Earthquake Research in China, 19(2), 132-147.

Liu, S., Zhang, J., Shu, G., Li, Q., 2005. Mineral chemistry, P-T-t paths and exhumation processes of mafic granulites in Dingye, Southern Tibet (in Chinese). Sciences in China (Serie D), 35(9), 810-820.

Lou, H., Wang, C., 2005. Wavelet analysis and interpretation of gravity data in Sichuan-Yunnan region, China (in Chinese). Acta Seismologica Sinica, 27(5), 515-523.

Lu, D., Cui, Z., Chen, J., 1989. Application of exploration seismic sounding in the study of the crustal structure of the Kangding-Dukou meridianal structural belt (in Chinese). Geological Review, 35(1), 41-51.

Ma, X., 1989. Lithospheric dynamics ATLAS of China. Beijing, China Cartographic Publishing House, 68pp.

Martí, A., Queralt, P., Jones, A.G., Ledo, J., 2005. Improving Bahr's invariant parameters using the WAL approach. Geophysical Journal International, 163, 38-41.

Medvedev, S., Beaumont, C., 2006. Growth of Continental Plateaus by Channel Injection: Constraints and Thermo-Mechanical Consistency. London, Geological Society, 268, 147-164.

Nelson, K.D., Zhao, W., Brown, L.D., 1996. Partially molten middle crust beneath southern Tibet: synthesis of project INDEPTH results. Science, 274, 1684-1687.

Peng, J., Zhou, X., 1991. Revierw on Chinese-United States bilateral workshop on Xianshuihe faults (in Chinese). International Earthquake Research, 7, 1-6.

Pham, V.N., Boyer, D., Therme, P., Yuan, X., Li, L., Jin, G., 1986. Partial melting zones in the crust in Southern Tibet from magnetotelluric results. Nature, 319, 310-314.

Renner, J., Evans, B., Hirth, G., 2000. On the rheologically critical melt fraction. Earth and Planetary Science Letters, 181, 585-594.

Rodi, W., Mackie, R.L., 2001. Nonlinear conjugate gradients algorithm for 2-D magnetotelluric inversion. Geophysics, 66(1), 174-187.

Roger, F., Calassou, S., Lancelot, J., Malavieille, J., Mattauer, M., Xu, Z., Hao, Z., Hou, L., 1995. Miocene emplacement and deformation of the Konga Shan granite (Xianshui He fault zone, west Sichuan, China): geodynamic implications. Earth and Planetary Science Letters, 130, 201-216.

Rosenberg, C., Handy, M.R., 2005. Experimental deformation of partially melted granite revisited: implications for the continental crust. Journal of Metamorphic Geology, 23, 19-28.

Royden, L.H., Clark, B., King, R.W., Wang, E., Chen, Z., Shen, F., Liu, Y., 1997. Surface deformation and lower crustal flow in eastern Tibet. Science, 276(5313), 788-790.

Schoenbohm, L.M., Burchfiel, B.C., Chen, L., 2006. Propagation of surface uplift, lower crustal flow, and Cenozoic tectonics of the southeast margin of the Tibetan Plateau. Geology, 34(10), 813-816.

Shen, Z., Lü, J., Wang, M., Bürgmann, R., 2005. Contemporary crustal deformation around the southeast borderland of the Tibetan Plateau. Journal of Geophysical Research, 110, B11409, doi:10.1029/2004JB003421.

Smith, J.T., Booker, J.R., 1991. Rapid inversion of two- and three-dimensional magnetotelluric data. Journal of Geophysical Research, 96(B3), 3905-3922.

Sun, J., Jin, G., Bai, D., Wang, L., 2003. Sounding of electrical structure of the crust and upper mantle along the eastern border of Qinghai-Tibet Plateau and its tectonic significance (in Chinese). Science in China (Serie D), 33(supplement), 173-180.

Sun, S., Jia, D., Hu, Q., 2007. Fluid inclusion planes measurement and paleostress field analysis for Cenozoic Gonggashan granite (in Chinese). Geological Journal of China Universities, 13(2), 344-352.

Swift, C.M., 1967. A magnetotelluric investigation of electrical conductivity anomaly in the southwestern United States. Doctoral thesis. Cambridge, Massachusetts Institute of Technology Massachusetts (USA), 1-211.

Teng, J., 1994. Rock physics and dynamics in Kangdian tectonic belt (in Chinese). Beijing, Science Press,1-13

Unsworth, M.J., Jones, A.G., Wei, W., Marquis, G., Gokarn, S.G., Spratt, J.E. and INDEPTH-MT team, 2005. Crustal rheology of the Himalaya and Southern Tibet inferred from magnetotelluric data. Nature, 438, 78-81.

Wang, C.Y., Han, W.B., Wu, J.P., 2007. Crustal structure beneath the eastern margin of the Tibetan Plateau and its tectonic implications. Journal of Geophysical Research, 112(B7), B07307, doi:10.1029/2005JB003837.

Wang, Y.Z., Wang, E.N., Shen, Z.K., Wang, M., Gan, W., Qiao, X.J., Meng, G.J., Li, T.M., Tao, W., Yang, Y.L., Cheng, J., Li, P., 2008. GPS-constrained inversion of present-day slip rates along major faults of the Sichuan-Yunnan region, China. Science in China Series D, 51(9), 1267-1283.

Wang, Z., Xu, Z., Yang, T., 1996. Study of the deformation mechanism of the Xianshui river fault zone: a shallow level, high temperature ductile shear zone (in Chinese). Regional Geology of China, 3, 245-251. (Please note: this journal only has series number for each year without volume's number)

Wei, W., Unsworth, M., Jones, A., Booker, J., Tan, H., Nelson, D., Chen, L., Li, S., Solon, K., Bedrosian, P., Jin, S., Deng, M., Ledo, J., Kay, D., Roberts, B., 2001. Detection of widespread fluids in the Tibetan crust by magnetotelluric studies. Science, 292, 716-718.

Wen, X., Yi, G., 2003. Re-Zoning of statistic units of seismicity in Sichuan-Yunnan region (in Chinese). Journal of Seismological Research, 26(supplement), 1-9.

Xu, X., Cheng, G., Yu, G., Song, F., Xiang, H., Zhang, L., Ron, H., Wang, Y., Wen, X., 2003. Tectonic and paleomagnetic evidence for the clockwise rotation of the Sichuan-Yunnan rhombic block (in Chinese). Seismology and Geology, 25(1), 61-70.

Xu, X., Wen, X., Yu, G., Zheng, R., Luo, H., Zheng, B., 2005. Slip rate, segmentation of surface rupture and earthquake recurrence of Litang fault zone, western Sichuan Province (in Chinese). Science in China (Serie D), 35(6), 540-551.

Xu, X., Wen, X., Ye, J., Ma, B., Chen, J., Zhou, R., He, H., Tian, Q., 2008. The Ms8.0 Wenchuan earthquake surface rupture and its seismognic structure (in Chinese). Seismology and Geology, 30(3), 595-629.

Xu, Z., Hou, L., Wang, Z., 1992. Orogenic processes of the Songpan-Gatze orogenic belt of China (in Chinese). Beijing, Geological Publishing House, 1-151.

Yuan, X., Li, T., Xiao, X., 2006. 3D lithospheric structure of the Qinghai-Tibet Plateau and hydraulic pressure machine model of the plateau uplift (in Chinese). Geology in China, 33(4), 711-729.

Zhan, Y., Zhao, G., Tang, J., Zhao, J., Jin, G., Deng, Q., Wang, J., 1999. Electric structure of the crust of Manas earthquake area in Xinjiang Autonous region (in Chinese). Seismology and Geology, 21(2), 159-167.

Zhang, P., Deng, Q., Zhang, G., Ma, J, Gan, W., Min, W., Mao, F., Wang, Q., 2003. Active tectonic blocks and strong earthquakes in the continent of China (in Chinese). Science in China (Serie D), 46(supplement), 13-24.

Zhang P., Xu, X., Wen, X., Ran, Y., 2008. Slip rates and recurrence intervals of the Longmen Shan active fault zone, and tectonic implications for the mechanism of the May 12 Wenchuan earthquake, 2008, Sichuan, China (in Chinese). Chinese Journal of Geophysics, 51(4), 1066-1073.

Zhang, Y., Chen, W., Yang, N., 2004. $^{40}Ar/^{39}Ar$ dating of shear deformation of the Xianshuihe fault zone in west Sichuan and its tectonic significance (in Chinese). Science in China (Serie D), 47(4), 794-803.

Zhang, Z., Klemperer, S.L., 2005. West-east variation in crustal thickness in northern Lhasa block, central Tibet, from deep seismic sounding data. Journal of Geophysical Research, 110, B09403, doi:10.1029/2004JB003139.

Zhao, G., Tang, J., Zhan, Y., Chen, X., Zhuo, X., Wang,J., Xuan, F., Deng, Q., Zhao, J., 2005. Relation between electricity structure of the crust and deformation of crustal blocks on the northeastern margin of Qinghai-Tibet plateau. Science in China Series D, 48(10), 1613-1626.

Zhao, G., Yukutake, T., Hamano, Y., Utada, H., Filloux, J., Law, L., White, T., Chave, A., Tarits, P., 1990. Investigation of magneto- variational data of the Juan de Fuca plate in the eastern Pacific Ocean (in Chinese). Chinese Journal of Geophysics, 33(4), 469-477.

Zhao, G., Chen, X., Wang, L., Wang, J., Tang, J., Wan, Z., Zhang, J., Zhan, Y., Xiao, Q., 2008. Evidence of crustal "channel flow" in the eastern margin of Tibetan Plateau from MT measurements. Chinese Science Bulletin, 53(12), 1887-1893.

Zhao, G., Chen, X., Xiao, Q., Wang, L., Tang, J., Zhan, Y., Wang, J., Zhang, J., Utada, H., Uyeshima, M., 2009. Generation mechanism of Wenchuan strong earthquake of Ms8.0 inferred from EM measurements in three levels (in Chinese). Chinese Journal of Geophysics, 52(2), 553-563.

Zhu, A., Xu, X., Zhou, Y., Yin, J., Gan, W., Chen, G., 2005. Relocation of small earthquakes in western Sichuan, China and its implications for active tectonics (in Chinese). Chinese Journal of Geophysics, 48(3), 629-636.

Zhu, J., Cai, X., Cao, J., Gao, D., Zhao, F., Du, Y., Wang, Y., 2005. The three-dimensional structure of lithosphere and its evolution in south China and east China sea (in Chinese). Beijing, Geological Publishing House, 1-186.

Zhu, S., Shi, Y., 2004.Genetic algorithm-finite element inversion of drag forces exerted by the 1ower crust on the upper crust in the Sichuan-Yunnan area (in Chinese). Chinese Journal of Geophysics, 47(2), 232-239.